THE JOURNAL OF BIOLOGICAL CHEMISTRY VOL. 286, NO. 4, pp. 2795–2806, January 28, 2011
Printed in the U.S.A.

Copper and Zinc Metallation Status of Copper-Zinc Superoxide Dismutase from Amyotrophic Lateral Sclerosis Transgenic Mice*[S]

Received for publication, September 24, 2010, and in revised form, November 5, 2010 Published, JBC Papers in Press, November 10, 2010, DOI 10.1074/jbc.M110.186999

Herman L. Lelie[‡], Amir Liba[‡1], Megan W. Bourassa[§¶], Madhuri Chattopadhyay[‡], Pik K. Chan[‡], Edith B. Gralla[‡], Lisa M. Miller[§¶], David R. Borchelt[‖], Joan Selverstone Valentine[‡2], and Julian P. Whitelegge[3]**

*From the [‡]Department of Chemistry and Biochemistry, UCLA, Los Angeles, California 90095, **The Pasarow Mass Spectrometry Laboratory, NPI-Semel Institute, David Geffen School of Medicine, UCLA, Los Angeles, California 90024, the [‖]Department of Neuroscience, Santa Fe Health Care Alzheimer's Disease Research Center, McKnight Brain Institute, University of Florida, Gainesville, Florida 32610, [§]National Synchrotron Light Source, Brookhaven National Laboratory, Upton, New York 11973, and the [¶]Department of Chemistry, Stony Brook University, Stony Brook, New York 11794*

Mutations in the metalloenzyme copper-zinc superoxide dismutase (SOD1) cause one form of familial amyotrophic lateral sclerosis (ALS), and metals are suspected to play a pivotal role in ALS pathology. To learn more about metals in ALS, we determined the metallation states of human wild-type or mutant (G37R, G93A, and H46R/H48Q) SOD1 proteins from SOD1-ALS transgenic mice spinal cords. SOD1 was gently extracted from spinal cord and separated into insoluble (aggregated) and soluble (supernatant) fractions, and then metallation states were determined by HPLC inductively coupled plasma MS. Insoluble SOD1-rich fractions were not enriched in copper and zinc. However, the soluble mutant and WT SOD1s were highly metallated except for the metal-binding-region mutant H46R/H48Q, which did not bind any copper. Due to the stability conferred by high metallation of G37R and G93A, it is unlikely that these soluble SOD1s are prone to aggregation *in vivo*, supporting the hypothesis that immature nascent SOD1 is the substrate for aggregation. We also investigated the effect of SOD1 overexpression and disease on metal homeostasis in spinal cord cross-sections of SOD1-ALS mice using synchrotron-based x-ray fluorescence microscopy. In each mouse genotype, except for the H46R/H48Q mouse, we found a redistribution of copper between gray and white matters correlated to areas of high SOD1. Interestingly, a disease-specific increase of zinc was observed in the white matter for all mutant SOD1 mice. Together these data provide a picture of copper and zinc in the cell as well as highlight the importance of these metals in understanding SOD1-ALS pathology.

First described in 1869 by French neurologist Jean-Martin Charcot (1), amyotrophic lateral sclerosis (ALS)[4] is defined by the progressive demise of lower and upper motor neurons leading to the degeneration of muscle tissue and eventual paralysis (2). Familial ALS was linked in 1993 to mutations in the gene that encodes the metalloenzyme copper-zinc, superoxide dismutase (SOD1) (3), and since that time more than 140 different disease-causing mutations have been identified (4). Before the discovery linking SOD1 and ALS, epidemiological studies on ALS suggested that exposure to metallic trace elements was a significant factor among many other environmental factors such as viruses, strenuous exercise, and excitotoxic chemicals that may have a role in ALS etiology (4–6). Studies on exposure to and tissue accumulation of metallic elements in ALS patients show a correlative yet unspecified role for many metals including copper and zinc in SOD1-related ALS (7–19). Over the years, a number of hypotheses relating metal toxicity to ALS have been proposed. For example, abnormal accumulations of redox-active metal ions such as iron or copper in ALS patients were generally believed to be detrimental due to their ability to mediate oxidative damage through participation in reactions that lead to formation of reactive oxygen species. A more specific hypothesis linking metallation levels of mutant SOD1 to ALS is that copper-replete but zinc-deficient forms of mutant SOD1 present *in vivo* could be responsible for toxicity via aberrant oxidative mechanisms (20). Metal ions, redox-active or not, could also interfere with normal protein function by binding to sulfhydryl (21), carboxylate, or amine groups of biomolecules (22). Abnormal levels of metal ions involved in synaptic transmission, signaling, and/or electrical transduction can also be detrimental. For example, ~10% of neuronal zinc is located in vesicles of glutaminergic neurons (23), and its release is important in neuromodulatory signaling. Consequently, excess zinc can be neurotoxic, making these neurons particularly sensitive to alterations in intracellular zinc levels (24). Calcium is also very important in synaptic transmission, and an influx of excess calcium ions into the neuron due to permissive glutamate receptors can result in glutamate excitotoxicity (25), which is observed as part of ALS pathology (26).

Recent studies have demonstrated that ALS-mutant SOD1 forms various types of oligomeric and aggregate structures *in*

* This work was supported, in whole or in part, by National Institutes of Health Grant P01 NS049134-01 (NINDS).

[S] The on-line version of this article (available at http://www.jbc.org) contains supplemental Figs. 1–5.

[1] Present address: Agilent Technologies, Wilmington, DE 19808.

[2] To whom correspondence may be addressed: Box 951569, 607 Charles E. Young Dr. East, Los Angeles, CA 90095-1569. Tel.: 310-825-9835; Fax: 310-206-9880; E-mail: jsv@chem.ucla.edu.

[3] To whom correspondence may be addressed: NPI-Semel Institute, David Geffen School of Medicine, UCLA, 760 Westwood Plaza, Los Angeles, CA 90024. Tel.: 310-206-7886; Fax: 310-206-2161; E-mail: jpw@chem.ucla.edu.

[4] The abbreviations used are: ALS, amyotrophic lateral sclerosis; SOD, superoxide dismutase; hSOD, human SOD; NTG, nontransgenic; ICP, inductively coupled plasma; XFM, x-ray fluorescence microscopy; hWT, human WT.

vivo (27–29). The formation of these structures is potentially modulated by the binding of metal cofactors to the mutant protein. Human wild-type (hWT) SOD1 in its fully metallated form is one of the most stable and soluble enzymes known, with a melting temperature above 90 °C and a long half-life (30). A large fraction of this thermal stability is due to binding of the copper and zinc ions (30–33), and several of the ALS-mutant SOD1 proteins are similarly stabilized by metal ion binding (4, 30, 33–35). The maturation of SOD1 involves three central features, the binding of a single copper and zinc to each subunit, a dimerization, and an intramolecular disulfide bond. Disruptions in these maturation steps may have relevance in SOD1 acquisition of toxic properties. For example, unmetallated (apo) SOD1 has far lower thermostability, melting at around 50 °C, and can be induced to form aggregates under a wide variety of conditions (36–40). These observations have led to the hypothesis that severe undermetallation of mutant SOD1 *in vivo* could be the principal cause of SOD1 oligomerization and aggregation (4, 41).

In the present study we examine the role of metals, in particular copper and zinc, in disease pathology using transgenic mice expressing mutant SOD1. Metal levels were measured in whole tissue and tissue subsections of ALS mice to better understand the changes in metal homeostasis associated with SOD1-mediated ALS. Our findings reveal significant changes in copper metabolism associated with SOD1 overexpression, with additional changes in zinc levels as disease progresses.

We have also analyzed the metallation of SOD1 in soluble and insoluble forms from the spinal cords of several lines of symptomatic mice, each expressing a different ALS-SOD1 mutant protein. In the spinal cords of mutant mice we show that soluble forms of mutant SOD1, with the exception of a mutant with a disrupted copper binding site, are highly metallated, whereas insoluble fractions from symptomatic mice showed no enrichment for copper or zinc. Collectively, these studies provide insight into the impact of mutant SOD1 expression on metal homeostasis and the role of metal binding in the generation of aggregated forms of mutant SOD1.

EXPERIMENTAL PROCEDURES

Mice—Nontransgenic (NTG) and transgenic mice expressing hWT, G93A, G37R, or H46R/H48Q hSOD1 were prepared and sacrificed as described in Wang *et al.* (42). Briefly, mice were sacrificed at the end stage of motor neuron degeneration when hind limb paralysis was pronounced or at age-matched times for the hWT and NTG controls. Brain, spinal cord, and liver were dissected for analysis. A total of 37 mice were analyzed in this study: 8 hWT, 8 G37R, 6 H46R/H48Q, 8 G93A, and 7 non-transgenic.

Whole Tissue Metal Content—Samples (20–25 mg) of liver, spinal cord, or forebrain were cut and weighed. The tissues were digested in 25 μl of a concentrated nitric acid solution for four h on a heat block set at 95 °C. Digests were diluted to 2 ml in 2% nitric acid, and total metal concentrations were determined using an inductively coupled plasma mass spectrometer (ICP-MS) (Agilent 7500) equipped with an autosampler (Cetac ASX 500).

Isolation of soluble SOD1—Based on procedures we had used in previous work for investigating soluble and aggregated SOD1 (43), we developed a new procedure to isolate intact, unaltered SOD1 from murine tissues without disrupting metallation levels. Spinal cord, brain, or liver samples were homogenized in 10 volumes of chilled, trace metal-free, phosphate-buffered saline (PBS), pH 7.4, using an ultrasonic disintegrator. Homogenate was centrifuged at 800 × *g* for 10 min (brain and spinal cord) or 4000 × *g* for 10 min (liver). Supernatants were loaded onto a gravity-flow G-75 size exclusion column. Soluble SOD1 eluted with about 75% purity. SOD1-containing fractions were identified by Western blot and, if necessary, concentrated before metallation analysis.

Isolation of Insoluble SOD1—Detergent-insoluble SOD1 was isolated by centrifugation as described previously (29, 43). Briefly, spinal cords were sonicated in 10 volumes of TEN buffer (10 mM Tris, pH 7.5, 1 mM EDTA, pH 8.0, 100 mM NaCl), and the homogenate was centrifuged at 800 × *g* for 10 min. This initial pellet, P1, was discarded, and detergent was added to the remaining supernatant to reach a concentration of 1% of Nonidet P-40. This sample was centrifuged at 100,000 × *g* for 1 h, and the resulting pellet, P2, was resuspended in 1 ml of TEN buffer with 0.5% Nonidet P-40, 0.25% SDS, and 0.5% deoxycholate, mixed, and centrifuged at 100,000 × *g* for 30 min. The resulting pellet, P3, was washed in the same buffer and re-centrifuged for 30 min at 100,000 × *g*. The washed P3 pellet was resuspended in 100 μl of trace metal-free PBS for storage and analysis.

Metal Concentration by ICP-MS—Metal concentration measurements on the detergent-insoluble pellets, whole cell homogenates, and tissues were run in the ICP-MS direct analysis mode. Samples were digested in 1:1 (v/v) concentrated nitric acid for 4 h and then diluted to 2 ml in 2% nitric acid solutions. An autosampler (ASX-500) loaded each sample into the ICP-MS, which was set to analyze the samples using the Octapole Reaction System using the hydrogen and helium modes. The intensities of the ions with a mass-to-charge ratio of 45, 52, 55, 56, 59, 63, 66, and 72 were measured, representing the metals scandium, chromium, manganese, iron, cobalt, copper, zinc, and germanium, with scandium and germanium serving as internal calibration standards.

Determination of Metallation State—To determine SOD1 metallation status, we used HPLC-ICP-MS (high pressure liquid chromatography coupled to an inductively coupled plasma mass spectrometer). Due to the novelty of this technique, details of the central aspects of this procedure are described below. After the crude, yet gentle isolation of SOD1 from mouse spinal cord homogenate, the samples were analyzed by HPLC-ICP-MS.

An high performance liquid chromatograph (Agilent 1200 series) with a size exclusion column (SW-2000, 7.8 × 300 mm, TOSOH Biosciences) was used to separate partially purified SOD1 from the majority of the contaminating species. The column was equilibrated and run isocratically with a mobile phase of 25 mM potassium phosphate, pH 6.7, 20 mM sodium chloride (trace metal free). The elution time for SOD1 protein off the column was ~15 min for most mutant SOD1s and ~16 min for the endogenous mouse SOD1, both eluting

well after the bulk of contaminating proteins, as monitored by the absorbance at 214 and 280 nm. The eluent stream was directed to the source of the ICP-MS using the high matrix interface (Agilent). ICP-MS analysis was run in the helium gas mode, with time-resolved analysis, to minimize signal suppression due to possible high salt content within the sample. The HPLC generated a chromatogram of the eluting proteins by monitoring the absorbance at 214 nm, and the ICP-MS generated trace chromatograms for copper, zinc, iron, and manganese concentrations from the ICP-MS ion extract signal. A signal in the 214-nm chromatogram at 15 min usually preceded a copper and zinc signal by 20 s, which is the time it takes the sample to get from the HPLC-diode array to the ICP-MS (supplemental Fig. 2). Supplemental Fig. 2 is an example of a G93A hSOD1 HPLC elution profile monitored by the 214-nm absorbance and the ICP-MS metal ion traces, with the base lines for manganese and iron blown up. As expected, neither iron nor manganese eluted with SOD1 in any of the samples analyzed. Analysis of a set of dilutions from known calibration standards was used to generate a standard curve. A linear regression analysis reveals a high correlation coefficient for SOD1 protein, copper, and zinc concentration measured by the HPLC-ICP-MS method compared with their known concentrations. (supplemental Fig. 3*A*). This procedure allowed us to calculate the precise concentrations of SOD1, copper, zinc, iron, and manganese for all unknown samples. The exact metallation state was then determined by dividing copper or zinc levels by the SOD1 concentration to yield the metal/dimer levels summarized in Fig. 2, *A–C*. All experiments were performed blind; the experimenter had no prior knowledge of the genotypes of the mice analyzed. At least three different mice, and in most cases five or more for each genotype, were analyzed. For each mouse, three or more replicates were analyzed to ensure accurate metallation state ($p < 0.05$, supplemental Fig. 3*B*). These data were then averaged across all mice of the same genotype to obtain the values displayed and the error shown. Hence the error shown is not the error of the measurements; rather, it represents the variability between mice of the same genotype.

Each type of SOD1 varied slightly in elution time off the HPLC size exclusion column. This turned out to be advantageous in the case of the H46R/H48Q mouse because the mouse SOD1 and the H46R/H48Q SOD1 from the same mouse lysate could be separately analyzed. H46R/H48Q human SOD1 elutes at 14 min, 2 min earlier than mouse SOD1.

To verify that the metallation states do not change before analysis due to cell lysis and protein isolation procedures, purified G93A SOD1 protein was added to a non-transgenic lysate, and metallation was determined before and after protein purification. The procedure did not change the metallation state for this control (data not shown).

Validation of SOD1, Copper, and Zinc Concentrations by Other Methods—The LC-ICP procedure returned three pieces of information simultaneously: SOD1 protein concentration by UV spectral trace and copper and zinc concentrations by ICP-MS ion trace. The concentration determined by LC-ICP was compared with that determined by the 214-nm absorbance measurement, Western blot densitometry, and the use of isotopically labeled peptides in a multiple reaction-monitoring experiment performed on an electrospray triple quadrupole mass spectrometer. Zinc and copper values were measured by simple ICP batch experiments. Copper levels were also estimated by SOD activity. Fig. 2*D* and supplemental Fig. 4 demonstrate the high degree of accuracy obtained by the LC-ICP method when compared with these other more conventional methods.

Activity Assays—SOD activity was measured using an assay based on inhibition of XTT reduction by superoxide (44). Samples were diluted into a xanthine oxidase solution (6 milliunits/ml) and then mixed with a solution containing 10 mM hypoxanthine, 5 mM XTT (sodium 3′-[(1-(phenylaminocarbonyl)-3,4-tetrazolium]-bis (4-methoxy-6-nitro) benzene sulfonic acid hydrate), and catalase (6000 units/ml). The rate of superoxide dismutation was calculated by the reciprocal rate of formazan formation as measured calorimetrically at an absorbance of 490 nm over 30 min.

SOD1 Concentration Determination by Selective Reaction Monitoring Mass Spectrometry—SOD1-containing samples were digested overnight by adding 1 μl of 1 μg/μl trypsin at 37 °C, with an internal standard consisting of two isotopically labeled synthetic SOD1 tryptic peptides. Peptide 1 (GDGPVQGIINFEQK) and peptide 2 (VGDLGNVTADK) had an isotopically labeled [^{13}C,^{15}N]lysine at the C terminus (Aqua-Thermo Scientific). Digested samples were loaded onto a reverse phase C4 column eluting to a triple quadrupole mass spectrometer (Q-trap 4000 Applied Biosciences) for selective reaction monitoring of the isotopically labeled peptides and their non-labeled counterparts in the sample. Quantification was based on the intensity of the internal labeled standards and a calibration set of human SOD1 with known concentration.

Spinal Cord Metal Distribution Imaging Analysis—Four of each end-stage mutant mice (G93A, G37R, and H46R/H48Q hSOD1) and age-matched control (hWT and NTG) were euthanized and perfused with trace metal-free PBS to remove blood from the vasculature. Spinal cords were fixed in 4% paraformaldehyde and soaked in 20% sucrose for improved sectioning. Twenty-micron-thick sections were cryosectioned and deposited on 0.5 μm-thick silicon nitride windows for FTIR imaging and x-ray fluorescence microscopy (XFM). To distinguish the white *versus* gray matter without staining, FTIR imaging was used. FTIR images were collected using a PerkinElmer Life Sciences Spectrum Spotlight infrared microscope in the mid-infrared region (4000 – 800 cm^{-1}) using a 6.25-μm pixel size, 8-cm^{-1} spectral resolution, and 8 scans co-added per pixel. The white and gray matter were distinguished from the FTIR images using unsupervised principal components analysis based on difference in lipid composition between these anatomical regions. After FTIR imaging, the copper and zinc contents were imaged in the same samples using XFM at beamline X27A at the National Synchrotron Light Source. X-ray fluorescence spectra were collected using an x-ray excitation energy of 11 keV and a beam size of 9 μm (vertical) × 17 μm (horizontal) in 15-μm steps, with an integration time of 7 s/pixel. The intensity for each metal was quantified by integrating the area under the curve for the re-

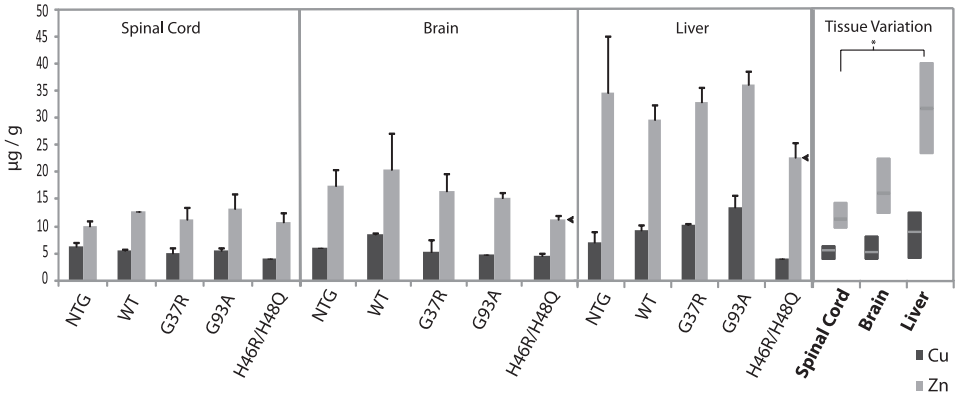

FIGURE 1. **Concentration of copper and zinc in whole spinal cord, brain, and liver reflect tight copper regulation.** Sections of spinal cord, brain, and liver from a NTG and transgenic mice overexpressing human WT, G37R, G93A, or H46R/H48Q SOD1 were weighed, completely digested in nitric acid, then subjected to metal quantitation by ICP-MS. The H46R/H48Q mouse brain and liver zinc concentrations were consistently lower than all other mice (*arrow*, $p < 0.005$). *Far right panel*, a box plot graph incorporating all measurements from the same tissue demonstrates that copper concentrations remain relatively constant in the brain and spinal cord, whereas zinc was lower in spinal cord, somewhat higher in brain (*p* value 0.019), and highest in liver (*, $p <$ 0.0001 relative to spinal cord). The *bar graph* results are reported in mean μg of metal/g of tissue (wet weight), and *error bars* represent $\pm$S.D. of three or more independent mice per genotype.

spective peak in the XRF spectrum (copper Kα = 8047.8 eV and zinc Kα = 8638.9 eV). National Institute of Standards and Technology thin film standard reference materials 1832 and 1833 were used to calculate concentration and to normalize for any differences between the multiple beamtime runs required to collect the data. The concentrations of zinc and copper in the standards were 3.75 and 2.52 μg/cm^2, respectively. To convert from μm/cm^2 to mM, the μm/cm^2 values were divided by the product of the volume of x-ray beam on the sample (area $\times$ thickness of the sample), the density of tissue (estimated to be 0.9 g/cm^3), and the molecular weight of the element.

Statistical Analysis of the XFM Data—The white and the gray matter in the spinal cord cross-sections were distinguished based on the principal components analysis of the FTIR images. The FTIR principal components analysis images were overlaid onto the zinc and copper XFM images, and masks were generated for the white and gray matter. Additionally, outlier pixels were identified as those pixels with a value >100$\times$ the median value and were excluded. Median values were calculated for both the gray and white matter of the copper and zinc maps.

All statistics were performed using SPSS Version 14.0. To test for significance within the regions of interest for the mutant, WT, and NTG mice, the Kruskal-Wallis test was performed on the medians for each group. Groups that satisfied $\alpha < 0.05$ were then subjected to post hoc analysis using the Mann-Whitney *U* test to determine the significance within the groups. A significance level of 0.05 was also used for the Mann-Whitney *U* test.

RESULTS

Overall Copper and Zinc Concentrations from Brain, Spinal Cord, and Liver

The intracellular concentrations of copper and zinc are tightly controlled at many levels (import, transportation, and export), and it was, therefore, unclear in advance what effect if any the transgenic overexpression of copper-zinc superoxide dismutase would have on total tissue copper and zinc concentrations. To determine whether the effects of disease and/or the overexpression of hSOD1 can affect overall metal concentrations within tissues, portions of the brain, spinal cord, or liver were subjected to ICP-MS for metal quantitation. The measurements were made on five different mouse types; three overexpressing SOD1 with the disease-conferring mutations G37R, G93A, and H46R/H48Q, one overexpressing WT hSOD1, and NTG mice. The G37R and G93A mutants are termed wild-type-like due to their similarity to wild-type hSOD1 with respect to metal binding properties (45), H46R/H48Q hSOD1 was constructed to combine two ALS- associated mutations in crucial copper binding residues (46).

The levels of copper and zinc in micrograms of metal per wet tissue weight in grams are shown in Fig. 1. Despite the up to 10-fold increased expression levels of hSOD1, the copper levels were relatively unchanged, varying between 4 and 6 μg of copper/g of wet tissue weight in the spinal cord. The mice expressing H46R/H48Q hSOD1, which does not bind copper (46), had the lowest copper levels at 4 μg/g. The NTG mouse had 6 μg/g of copper in the three tissues. The G37R, G93A, and WT SOD1 transgenic mice had only 5 μg/g of copper in the spinal cord and brain despite the fact that these SOD1 mutants are known to have a high copper binding capacity (30, 47). The low variability in copper concentrations within each tissue reflects the tight regulation of this metal (Fig. 1, *right panel*). Liver, however, was the exception. In mice expressing an SOD1 capable of binding copper (G37R, G93A, and WT), copper in the liver was significantly higher than the other tissues at 9, 10, and 13 μg/g, respectively (Fig. 1). This observation may be related to the function of liver for storing excess copper, which may allow for a larger window of copper concentrations (48). Aside from the elevated copper content in the G37R, G93A, and WT livers, total tissue copper levels were generally independent of SOD1 mutant expression levels and remained consistent in the spinal cords and brains across the different types of mice (Fig. 1, *right panel*).

Biological zinc levels are generally higher than those of copper (49, 50). Fig. 1 shows that zinc concentrations vary significantly across the different mouse tissues, with the highest lev-

els in the liver. It has been suggested that the liver participates directly in zinc metabolism, and the liver is known to serve as a storage site for excess zinc. Accordingly, a dramatic range of zinc concentrations has been observed in that tissue (51). Within the spinal cord, zinc concentrations were the lowest, brain was slightly higher, but liver had more than double the concentration of zinc than the spinal cord (Fig. 1, *right panel*) (p value <0.0001). Zinc concentrations within individual tissues also appeared to be significantly affected by transgenic SOD1 expression. The H46R/H48Q mouse, which overexpresses an SOD1 with a lower zinc affinity than the other transgenic SOD1s (46), appeared to consistently have the lowest overall zinc concentration relative to other genotypes (p value 0.004 brain, 0.3 spinal cord, 0.0001 liver), whereas the G93A and/or hWT mice appeared to have the highest levels of zinc in each tissue analyzed (p value 0.04–0.08). To ensure that our results were consistent with those of earlier studies, the metal concentrations from our NTG mice were compared with previously reported values from the literature. All values reported here are well within the range of previously reported values for nontransgenic mice (supplemental Fig. 1) (52–58).

The levels of several other metal ions, iron, manganese, chromium, calcium, and cobalt, were determined simultaneously and are shown in supplemental Fig. 5. These metal ions did not reveal any measurable alterations among the different mice strains. However, manganese appeared to have increased levels in mutants compared with the controls, but the difference did not reach statistical significance (NTG and hWT both had 0.45 μg/g, whereas mutants ranged between 0.51 and 0.6 μg/g, p value 0.17). Interestingly, previous reports have shown increases in manganese concentrations in ALS patient tissues (13).

Collectively, these results show that copper concentrations are held constant in the brain and spinal cord and are essentially independent of SOD1 concentration. Zinc levels, on the other hand, vary depending on the tissue and are partially influenced by the type and concentration of SOD1 present.

SOD1 Metallation States from Mouse Tissues

SOD1 Metallation States from Mouse Spinal Cord—A new procedure for measuring the *in vivo* metallation state of SOD1 isolated from mouse spinal cord is detailed under "Experimental Procedures." Briefly, this involved a gentle one-step size exclusion chromatographic purification of SOD1 from spinal cord homogenate followed by direct in-line analysis on an HPLC-ICP-MS. By this method we separated SOD1 from other proteins and measured protein, copper, and zinc concentrations on the eluent of the HPLC column. Fig. 2*A* shows the copper and zinc contents of soluble hSOD1 from the spinal cords of WT, G37R, G93A, and H46R/H48Q transgenic mice and of endogenous mouse SOD1 from the nontransgenic mouse. The H46R/H48Q mutant SOD1 did not bind any copper *in vivo* as was intended by its design and consistent with previous *in vitro* studies (13, 29) (46). Zinc metallation values for H46R/H48Q mice varied between individual mice, as indicated by the large error bars, but they were consistently lower than the metallation values of the other transgenic SOD1s (hWT, G37R, and G93A; p value 0.0003), corroborating previous *in vitro* biophysical studies that showed that this mutant has greatly reduced affinity for zinc (46). For the other transgenic SOD1s (hWT, G37R, and G93A), the metallation status was fairly constant at ~1–1.25 copper per dimer and 2.6–3.2 zinc per dimer. Interestingly, the metallation results shown in Fig. 2*A* and summarized in Fig. 2*E*, *right panel*, are similar to those of as-isolated hSOD1 proteins overexpressed in various host organisms such as from insect cells and *Saccharomyces cerevisiae,* where copper varied between 0.5 and 1.5 and zinc varied between 2 and 3 per dimer (45).

In general, the metallation status of hSOD1 in the hSOD1 transgenic mice is considerably different from that of the endogenous mouse SOD1 in the NTG mouse. In the latter case, the copper and zinc levels are roughly two copper ions and two zinc ions per dimer (or one of each per subunit), and copper and zinc are present in a ratio of ~1:1. Fig. 2*A* demonstrates that the SOD1 from mice overexpressing active SOD1s (G93A, G37R, and hWT) show a shift in the ratio of copper to zinc to 1:3. Interestingly, human WT-SOD1 had an even slightly lower copper content compared with the mutant SOD1s G93A and G37R and a small but statistically significant elevation in zinc content (*).

One of the most unexpected discoveries was that soluble G93A and G37R had a combined copper and zinc metallation very close to four, which is equivalent to the total number of copper and zinc binding sites in an SOD1 dimer, implying strongly that the soluble proteins reached maximum metal occupancy (~98–99%) (Fig. 2*E*). A similarly high *in vivo* metallation state was observed across the different tissues analyzed (Fig. 2*E*). Generally, soluble human WT SOD1 had the highest total metallation, whereas soluble mouse SOD1 isolated from a NTG mouse had an ~85–100% metal site occupancy. Interestingly, the soluble H46R/H48Q hSOD1 only had ~25% metal occupancy, revealing that a wide spectrum of SOD1 metallation states can exist in soluble SOD1 *in vivo*.

Brain and Spinal Cord SOD1 Have Similar Metallation Levels—To determine whether the altered SOD1 metallation states are specific to the spinal cord, SOD1 was purified from mouse brains (without the brainstem) and subjected to the same SOD1 metallation analysis. Despite the lack of evidence of disease in this tissue, the soluble SOD1 metallation levels were very similar to those found in the spinal cord (Fig. 2, *B* and *E*). Metal ratio trends were similar as well, with higher zinc and lower copper bound to hWT compared with the wild-type-like mutants G37R and G93A. The variable zinc metallation for H46R/H48Q SOD1 was also observed in the brain SOD1.

Metallation Trends in Liver Differ from Those in Neuronal Tissues—We measured the metallation profile of soluble SOD1 isolated from a non-neuronal tissue, that is, the liver (Fig. 2*C*), and found significantly different metallation levels. Generally, the transgenically expressed SOD1s had lower total metal occupancy in liver than in nervous tissue. The endogenous mouse SOD1 from NTG mice maintained close to a one copper to one zinc ratio in each tissue measured; however, the mouse SOD1 in liver had the highest overall levels of both

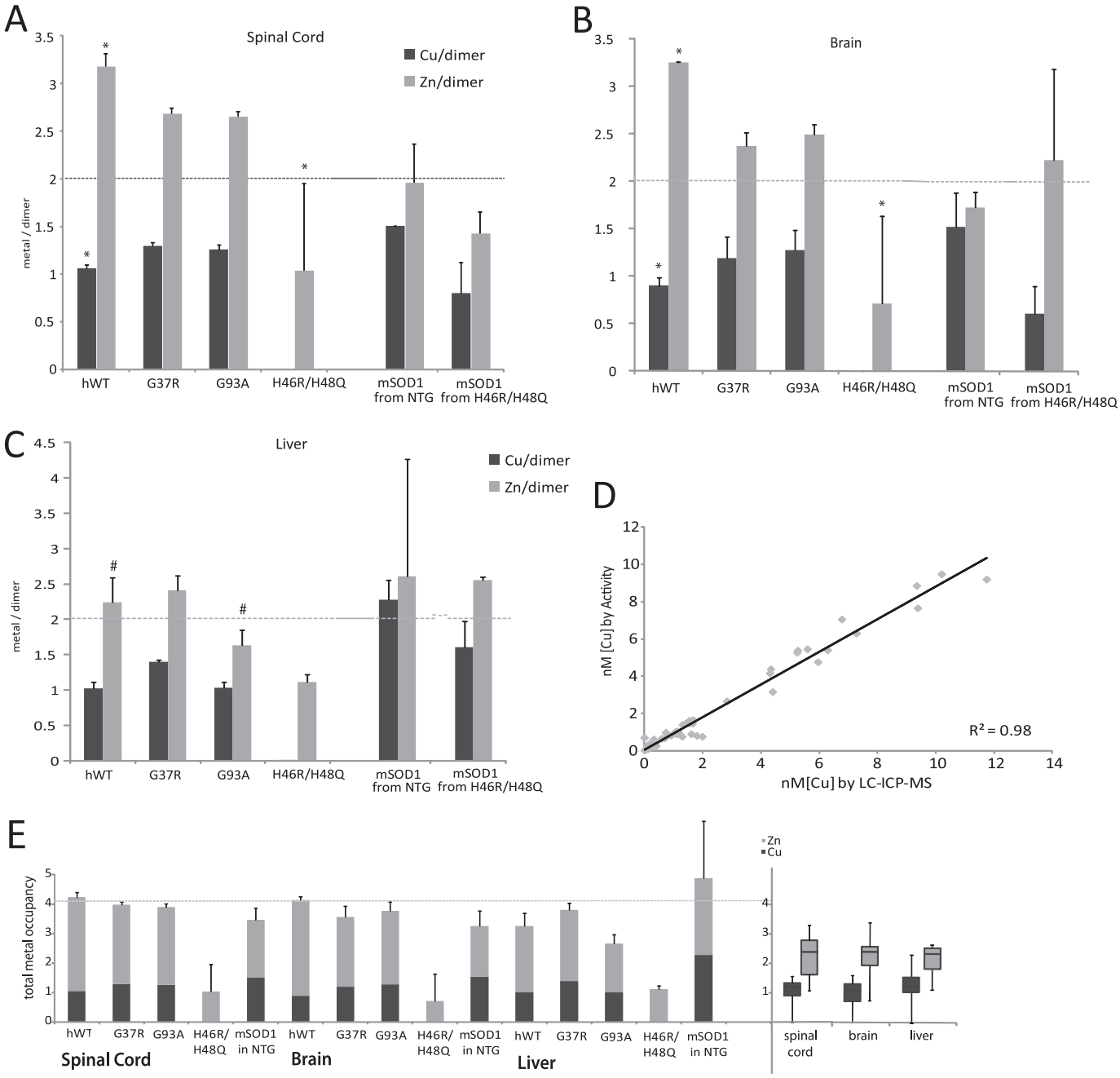

FIGURE 2. **SOD1 metallation in various tissues from transgenic mice.** Copper and zinc in SOD1 was measured by HPLC-ICP-MS as described under "Experimental Procedures." The metallation of WT, G37R, G93A, and H46R/H48Q hSOD1 from transgenic mice and the endogenous mSOD1 from a nontransgenic mouse are shown. *A*, spinal cord is shown. *B*, brain is shown. *C*, liver is shown. Note that in spinal cord and brain the total metal site occupancy does not differ significantly for the G37R, G93A, or hWT SOD1 or the mouse SOD1. However, the copper and zinc ratios are different, with less copper and more zinc being found in the overexpressed human SOD1s as compared with mouse SOD1 in the non-transgenic animals. Human WT-SOD1 had a slightly lower copper content and a higher zinc content compared with the mutant SOD1s G93A and G37R (*). The mutations in H46R/H48Q SOD1 destroy the copper binding site, and as such no detectable copper levels were found. Zinc metallation is also significantly lower in the H46R/H48Q mutant compared with the other transgenic SOD1s (*). In liver, SOD1 metallation is starkly different; in particular, G93A and hWT had dramatically reduced zinc occupancy levels relative to nervous tissue (#). *D*, the coppers bound to the SOD1 are active. A plot of the copper concentrations measured by the HPLC-ICP method compared with the copper measured by SOD activity shows a strong correlation, which indicates that the majority of copper bound to these SOD1 species are active. The measurements are from all the endogenous and exogenously expressed SOD1s from the mice analyzed in this study. *E*, *right*, shown is a *stacked bar graph* representation of metallation to illustrate total metallation. The *dashed line* at four metals/dimer delineates a fully occupied metal binding site. With the exception of the H46R/H48Q mutant, most other SOD1s are highly metallated. *Left*, shown is a *box plot graph* of combined metallation states for each tissue demonstrating tissue variability. Despite the vastly different trends among mutant metallation states, it is interesting to note that median copper and zinc values remain consistent across all tissues examined; these are also similar to as-isolated SOD1s from various host organisms. All *bars* represent the mean ± S.D. of three or more independent mice per genotype. *Box plots* represent median values and 25th to 75th percentile ranges. * $p < 0.001$; # $p < 0.01$.

copper and zinc per dimer. The soluble H46R/H48Q mutant still did not bind copper, whereas zinc metallation exhibits less variation among replicates of the same genotype. Furthermore, G93A and hWT had dramatically reduced zinc occupancy levels relative to nervous tissue (p value < 0.01), suggesting that the phenomenon of "excess" zinc binding may

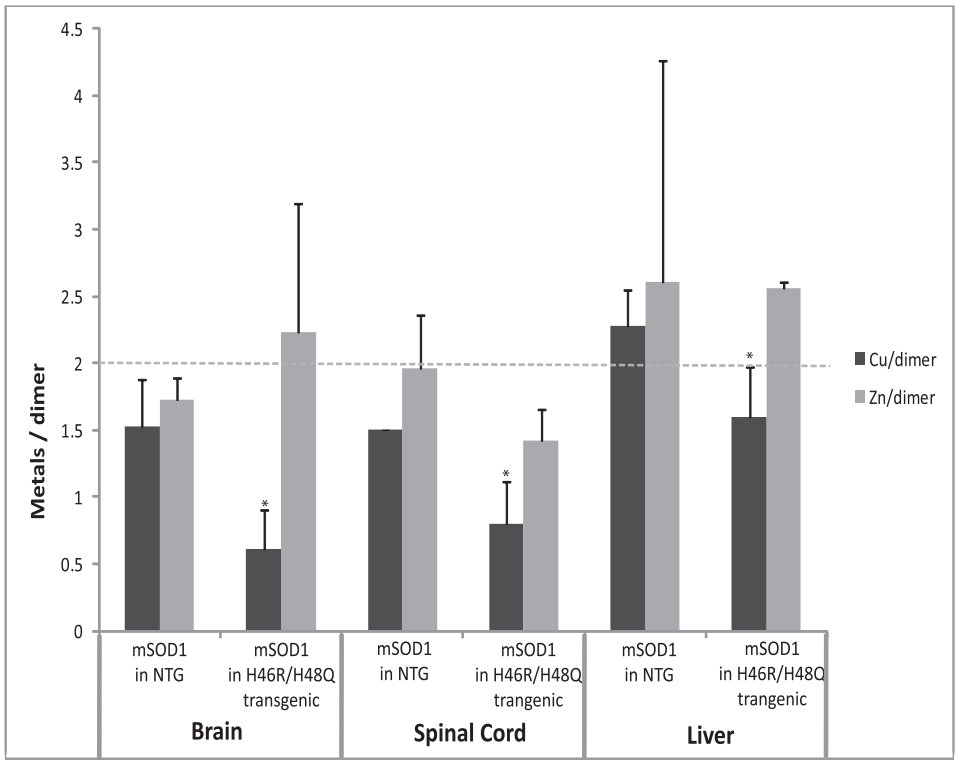

FIGURE 3. **Transgenic expression of a H46R/H48Q SOD1 results in decreased copper metallation of the endogenous mouse SOD1.** The metallation states of mouse SOD1 from a non-transgenic and transgenic mouse are shown. The metallation state of mouse SOD1 was measured from the brain, spinal cord, and liver of a nontransgenic and a H46R/H48Q transgenic mouse. Because the H46R/H48Q SOD1 mutant protein eluted differently from the mouse SOD1 off the HPLC column and does not bind copper, it was possible to measure the effect of overexpression separated from effects of insufficient copper. Overexpression of this hSOD1 leads to decreased copper metallation for the mouse SOD1 as inferred when comparing mSOD1 in NTG to mSOD1 in H46R/H48Q (*) for each tissues examined. *, $p < 0.05$.

pertain more to nervous tissue. The major shift in metallation compared with spinal cord and brain highlight the differences in tissue types.

Copper Is Properly Bound and Participates in the SOD Reaction for all Soluble SOD1—Copper is capable of binding to other sites on hSOD1 (45, 59), To determine whether the copper observed in this study was correctly bound in the active site, an SOD activity assay was performed on all samples. Because copper participates directly in the dismutase reaction, the overall activity is strictly dependent on the amount of copper bound to the active site (60). A plot of copper concentration measured by the LC-ICP method *versus* copper concentration calculated from the activity reveals a linear correlation with a slope near one (Fig. 2*D*) and a high correlation coefficient of 0.9751. Thus, the copper associated with SOD1 is active in the SOD assay and, therefore, may be assumed to be correctly bound to the copper binding site.

Effect of Transgenic Expression of the Mutant Human SOD1 H46R/H48Q on the Metallation of Endogenous Mouse SOD1—Because of the high sensitivity of the HPLC-ICP method, we were able to analyze metallation levels of endogenous mouse SOD1 from NTG mice. In addition, the difference in the elution time from the size exclusion column between the H46R/H48Q mutant hSOD1 and endogenous mouse WT SOD1 allowed us to analyze the metallation states of each of these proteins separately and to investigate the effect of overexpression of a mutant hSOD1 on the metallation status of endogenous mouse SOD1. Fig. 3 shows the copper and zinc metallation of mouse SOD1 from spinal cord, brain, and liver of both the NTG and H46R/H48Q transgenic mice. In all tissues, the copper-site occupancy in the mouse SOD1 was reduced when H46R/H48Q hSOD was expressed. Zinc metallation was not affected. Thus, we predict that the transgenic expression of mutant hSOD1 can significantly perturb the metal loading of the endogenous mouse SOD1, leading to a consistent reduction in copper occupancy, even in a mutant such as H46R/H48Q hSOD1 that does not bind copper ions at the copper site.

Insoluble Aggregates from Mutant Mice Are Not Enriched in Copper or Zinc

It is important to determine the metallation state of SOD1 in the aggregated state as these protein aggregates may be related to the toxic species. Mutant SOD1 in the apo state has dramatically decreased thermostability and, hence, increased aggregation propensity, and it has, therefore, been hypothesized that insoluble aggregates of mutant SOD1 are composed of metal-depleted SOD1 (38, 40). Differential detergent extraction and centrifugation techniques were used to separate the mutant SOD1 aggregates that accumulate as disease symptoms worsen (28, 29, 61, 62). Because the aggregated protein cannot be easily dissociated, it was not possible to isolate specifically the SOD1 protein in these fractions for ICP analysis. Instead, the total metal content of these detergent-insoluble pellets was measured by ICP-MS, and the amount of mutant SOD1 protein was measured by densitometry of a

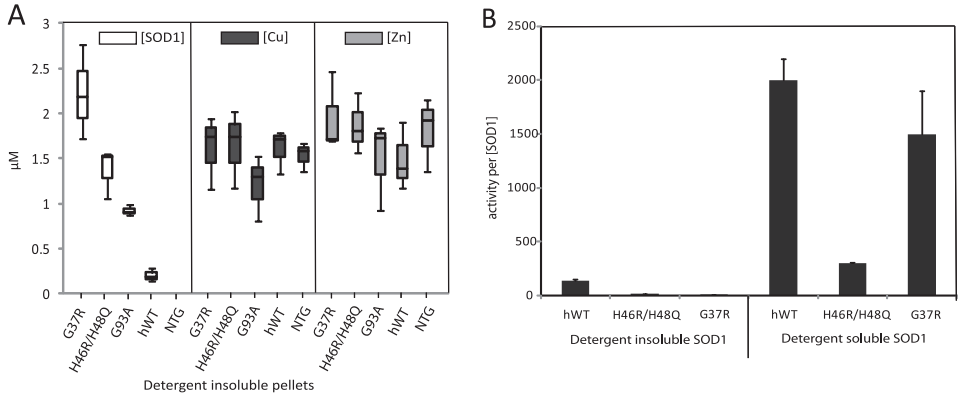

FIGURE 4. **Copper and zinc concentrations from detergent-insoluble and -soluble species suggest minimal SOD1 metallation in detergent-extracted SOD1.** *A*, the detergent-insoluble species were prepared from nontransgenic and G93A, G37R, H46R/H48, and hWT SOD1 transgenic mice. SOD1 concentration was measured by densitometry from a Western blot, and the copper and zinc concentrations were measured by ICP-MS. Despite the variable levels of SOD1 from each detergent insoluble pellet preparation, the levels of copper and zinc did not fluctuate across all the mice types. *B*, detergent-insoluble and detergent-soluble species were analyzed for activity and SOD1 concentration. The relative activity was divided by the SOD1 concentration to gain a rough idea of the level of copper bound to the SOD1. The *axis on the left* is in arbitrary units. The soluble hWT, H46R/H48Q, and G37R SOD1s were measured as 2123, 172, and 1682, respectively, which was significantly higher activity per dimer than their detergent-insoluble counterparts, which measured as 143, 9, and 18, respectively. Note that very little WT hSOD1 was found in the detergent-resistant pellets. The *box plots* represent median values and 25th and 75th percentile ranges, and *bar graphs* represent mean ± S.D. of three or more independent mice per genotype.

Western blot. SOD1 comprises about 4–6% of total protein in these pellets. These data allowed us to estimate roughly the ratio of total metal ions to SOD1 protein present in the pellets. The detergent-resistant pellets from spinal cords of NTG and hWT SOD1 transgenic mice did not contain significant amounts of SOD1 but do have a profile of other proteins similar to that found in spinal cords of mutant-expressing mice (43), making them good controls for the background concentration of metals from other metal-binding proteins. The concentrations of SOD1, copper, and zinc from detergent-insoluble pellets were plotted for each mouse type (Fig. 4*A*). On a molar basis, these prepared samples had more copper and zinc than SOD1, indicating that metals were bound to other insoluble components of these preparations. Importantly, the insoluble material from mutant mice did not contain more copper or zinc than insoluble material from mice expressing WT SOD1 or nontransgenic mice. We, therefore, conclude that mutant SOD1 is not a major copper or zinc binding component of these insoluble fractions.

To assess the levels of copper bound to the native copper site of SOD1, an SOD activity assay was performed on the detergent-insoluble pellets. The activity of these samples was divided by the total concentration of SOD1, and the results compared with those for the soluble SOD1 activity (Fig. 4*B*). The activity per molecule was very low in the mutant SOD1 from pellets, consistent with our conclusion that very little copper was associated with the copper binding site of these mutant SOD1s.

To control for the possibility that the copper may have been released when SOD1 was exposed to the non-ionic detergents during the extraction protocol, purified G37R hSOD1 was incubated in extraction buffer, and its metallation was measured before and after exposure. The metallation levels did not change (data not shown), confirming that the isolation procedure does not lead to the loss of active site copper in the insoluble SOD1 detergent-resistant pellets. Further studies are still required to confirm directly that SOD1 is metal-depleted. Nevertheless, these results are consistent with the idea that insoluble mutant hSOD1 is deficient in both copper and zinc.

Distribution of Metals in Spinal Cord Tissues

The HPLC-ICP analyses on soluble hSOD1 from mouse tissues suggest that both the nature of the mutation and the expression level affect metal occupancy, but they provide no information about distribution of metals in sub-tissue regions or different cell types. The perturbations in metal occupancy could lead to disturbances in whole tissue metal concentrations, which could be detrimental to the animal. Conversely, altered metal homeostasis may influence the metallation state of the SOD1 through changes in available pools. To address this matter more directly, the distribution of copper and zinc in spinal cord cross-sections of transgenic and control mice was determined using XFM.

To establish the location of the white matter, gray matter, dorsal horn, and ventral horn without staining, FTIR imaging was first performed on spinal cord cross-sections. Principal component analysis based on the lipid region of the infrared spectrum revealed deep contrast between the white *versus* gray matter and ventral *versus* dorsal horn (Fig. 5*A*, *top row*). The *white* and *gray areas* reflect the white and gray matter, respectively, the *left gray matter* lobe represents the ventral horn, and the *right gray matter* lobe represents the dorsal horn. Motor neuron cell bodies originate in the ventral horn of the gray matter and descend their tracks through the surrounding white matter. Some of these tracks are visible as streaks across the white matter in the FTIR images.

Copper and zinc distribution were determined by XFM on the identical tissue sections (Fig. 5*A*, *center* and *bottom row*, respectively). Fig. 5*A* shows a representative cross-section from each mouse type. The different types of mutants showed distinct results. In samples from mice that overexpress metal binding SOD1s (WT, G93A and G37R), the copper concentration increased within the gray matter. The H46R/H48Q

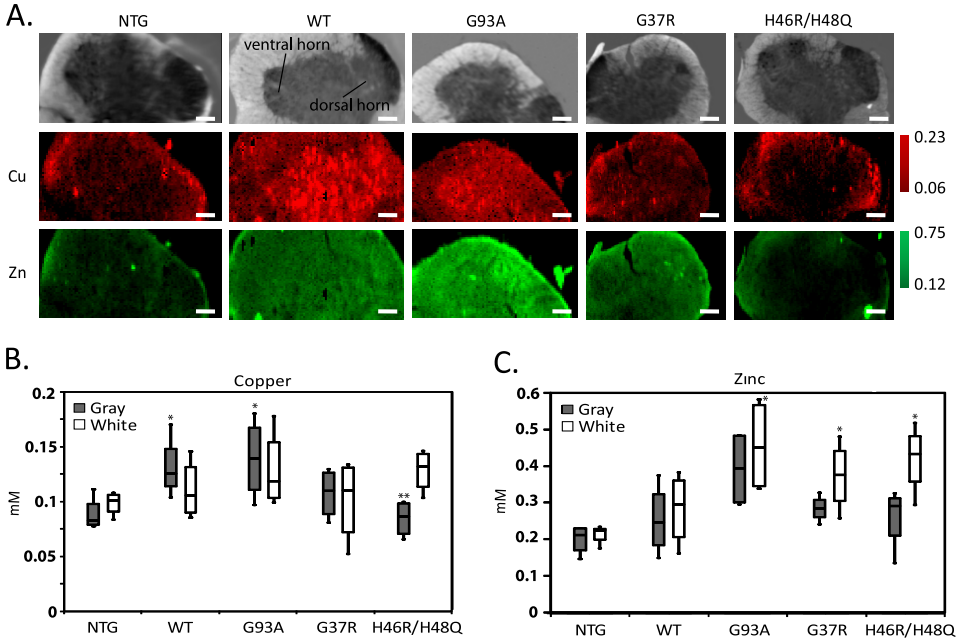

FIGURE 5. **Infrared and x-ray fluorescence microscopy images data analysis of spinal cord cross-sections from NTG mice or mice expressing WT, G93A, G37R, or H46R/H48Q SOD1.** *A*, image maps prepared from infrared and x-ray fluorescence data collection are shown. *Top row*, principal component analysis of the infrared images clearly differentiates between the white and gray matter based on differences in lipid and protein composition. The copper (*middle row*) and zinc (*bottom row*) XFM images illustrate changes in metal concentration and distribution as a function of SOD1 expression and mutation state. XFM images are presented in micromolar units as determined by the NIST standard reference. The *scale bar* represents 0.1 mm. At least three cross-sections were analyzed from four mice of each genotype, and representative images are shown. *B*, median copper and zinc concentrations (mM) in the same cross-sections of spinal cord, as measured by XMF are shown. All spinal cords from mice expressing mutant hSOD1 showed elevated zinc in the white matter as compared with NTG. In the gray matter, copper was elevated over NTG in WT, G37R, and G93A but not in the double mutant H46R/H48Q, which does not bind copper (*, significantly different from NTG; **, significantly different from WT by Kruskal-Wallis and Mann-Whitney *U* test). At least three cross-sections were analyzed from four mice of each genotype.

and the NTG mice, which have very low SOD1 copper metallation and low SOD1 levels, respectively, show much lower copper content in the gray matter. Zinc, on the other hand, was higher in the mutants than the NTG control and was consistently higher in the white *versus* gray matter for all samples analyzed. An increase in zinc associated with white matter was previously detected by XFM on cerebellum tissue cross-sections. It was postulated that this increase may be due to the requirement for zinc in myelin synthesis, structure, and maintenance (63).

A quantitative analysis of copper and zinc was performed by separating pixels from the gray and white matter and performing statistical analyses as a function of tissue substructure and mutation state (see "Experimental Procedures"). Statistically significant increases in gray matter copper were observed between NTG *versus* G93A and WT mice (*) and between WT *versus* H46R/H48Q mice (**), confirming the observation described above (Fig. 5*B*). The expression of SOD1 was reported to be higher in gray matter than white matter (64), which could explain the elevated copper levels in transgenic mice that overexpress copper binding SOD1. The major zinc trend did not reflect metallated SOD1 expression. Intriguingly, the symptomatic G37R, G93A, and H46R/H48Q mice (*) had statistically significantly elevated levels of zinc relative to the control NTG mice in the white matter, possibly reflecting a phenomenon that may be associated with disease pathology rather than with overexpression of the mutant protein itself (Fig. 5*C*).

DISCUSSION

The metals copper and zinc are integral to SOD1 structure and function and, hence, may play a role in ALS pathology. In the current investigation we study their distribution at the tissue, subtissue, and protein levels. We found that although increasing expression of SOD1 did not lead to an overall increase in spinal cord metal content, there was a subtle redistribution of copper into gray matter relative to white matter that is consistent with the idea that motor neurons produce more SOD1 than surrounding cells. These investigations also provide the most precise quantification available to date of metallation status in SOD1 from spinal cord, brain, and liver. Although the data from insoluble protein are consistent with insoluble SOD1 not binding copper and zinc, the soluble SOD1s reveal a significantly high degree of zinc binding and somewhat lower copper binding, suggesting that a significant fraction of soluble hSOD1 in mice is enzymatically inactive. Finally, this study provides verification that the H46R/H48Q mutant SOD1 does not bind copper *in vivo*, and therefore, disease for this mutant is not a result of copper-mediated chemistry.

The determination of *in vivo* SOD1 metallation states provides insight into the physiologically relevant and possibly disease-relevant species. The H46R/H48Q mutant averaged ~1.0 zinc per dimer, whereas the hWT, G93A, and G37R retained 2.6–3.2 zinc per dimer. This relatively high level of zinc binding is inconsistent with previous hypotheses regard-

ing a pathogenic zinc-deficient mutant SOD1 (65). We also believe that these zinc ions are likely to be bound to SOD1 in the zinc and copper sites because the total metallation does not ever exceed four metal ions per dimer, in opposition to theories invoking improper metal binding outside the metal binding region. Moreover, based on the instances where the zinc levels are above two per dimer, we further conclude that the zinc is bound in the copper site for some SOD1s.

A major question we hoped to address from these studies was whether low metallation of mutant SOD1 was linked to aggregation. However, the similarity between the WT and G37R and G93A mutants in metallation of soluble SOD1 in end stage mice is not consistent with the notion that under-metallation of these mutants causes aggregation. A possible explanation may be that our analysis is biased toward soluble SOD1, and hence, only stable, highly metallated species persist. However, the H46R/H48Q mutant remained soluble despite low metallation, which implies that a mutant SOD1 can remain soluble *in vivo* even if it does not have its full complement of metals and only binds one zinc per dimer. When we take into account the similarity in SOD1 metallation states between the affected spinal cord and unaffected brain tissue, we conclude that the lack of proper metallation is a minor factor in disease and aggregation. Furthermore, we hypothesize that the soluble mutant G93A and G37R hSOD1 from spinal cord analyzed here is unlikely to aggregate or play a role in any toxic aggregation mechanism, and the high levels of metallation in these soluble SOD1s likely protect SOD1 from aggregating.

Copper Metallation and Disulfide Oxidation—Aside from the relevance to aggregation, metallation states data can render important clues about the SOD1 maturation pathway. For instance, copper metallation has been suggested to occur concomitant with disulfide bond formation *in vivo* (66). Interestingly, copper binding follows a trend similar to that observed by Karch *et al.* (67) for disulfide oxidation; mouse SOD1 from NTG mice had the highest ratio of oxidized to reduced disulfide bonds followed by the G93A, then hWT, and finally, the H46R/H48Q. We see a direct correlation to copper metallation where the mouse SOD1 from NTG had the highest copper metallation followed by G93A, then hWT, and finally, the H46R/H48Q. This finding supports the idea that copper metallation and disulfide oxidation may be linked post-translational events.

Interestingly, an inverse relationship exists between copper and zinc metallation levels in SOD1 as well; *i.e.* when copper levels were lower, zinc levels were higher. The mouse SOD1 from the NTG spinal cord had metallation levels of ~1.5 copper and 2.0 zinc per dimer, close to what is expected for "normal" SOD1 (2 copper, 2 zinc). The mutants G93A and G37R both had lower copper (1.2 copper per dimer) and higher zinc (2.6 zinc per dimer). The hWT has even lower copper (1.0 copper per dimer) and even higher zinc (3.2 zinc per dimer) than the mutants (see Fig. 2*E*). This trend combined with the assumption that the extra zinc present in SOD1, when zinc levels exceed 2.0 per dimer, is in the copper site, suggests that copper and zinc metallation are linked. In physiological situations, it is entirely possible that zinc is bound to the copper site before copper insertion (68). It is interesting in this respect to note that SOD1 containing 4.0 zinc per dimer has been shown to be highly stable, similar to the properly metallated two-zinc and two-copper form (69).

Perturbations in Metallation of SOD1 Caused by Transgenic Overexpression of hSOD1—Several lines of reasoning lead us to believe that over-burdened copper regulation pathways are responsible for the observed perturbations in SOD1 metallation by copper. First, as demonstrated by the whole tissue analysis, copper levels in tissues do not change significantly in the different types of mice despite overexpression of SOD1. Moreover, the hWT SOD1 has the highest overall expression (7–10-fold endogenous levels) and longest half-life among the transgenically expressed SOD1 (70) and, therefore, has the highest demand for copper. Correspondingly, WT hSOD1 was isolated with the lowest copper metallation. A limited pool of copper and a swamped insertion pathway may be responsible for the reduced copper charging. Even more strikingly, we observed a consistent decrease in copper metallation of the endogenous mouse SOD1 from the H46R/H48Q-overexpressing mutant compared with mouse SOD1 from the NTG (Fig. 3). We hypothesize that, although the H46R/H48Q mutant does not bind copper itself, it does interfere with copper insertion pathways such as the copper chaperone for SOD1 (CCS), possibly restricting copper acquisition for the endogenous mouse SOD1. The H46R/H48Q mutant is known to form stable heterodimers with the copper chaperone, CCS, possibly limiting the rate of copper insertion in the mouse SOD1 (46). Together, these data suggest that incomplete maturation of SOD1 with respect to copper insertion is a result of overexpression of the SOD1s.

Implications for SOD1 Aggregation Mechanisms—Our studies suggest that insoluble SOD1-containing species are not enriched with copper and zinc, consistent with the idea that the aggregated SOD1 is metal-depleted. However, more direct studies are needed to confirm this hypothesis. Nevertheless, we found that the soluble forms of mutant SOD1 isolated from spinal cord are fully, but not natively, metallated, containing four metal ions per dimer. Although it is possible that a metallated SOD1 could enter an aggregate and subsequently lose its metals, that scenario seems unlikely to us due to the high stability of some of the fully metallated forms of mutant SOD1s. It seems more likely that it is the apo forms of mutant SOD1s that form aggregates. A possible explanation for this apparent contradiction is that nascent SOD1 polypeptides, which have not yet been metallated, are the main substrates for aggregation. Support for this hypothesis is provided in the earlier analysis of SOD1 aggregates, which revealed that the SOD1 protein was largely unmodified (43). Unpublished results from our laboratory show that soluble SOD1 in spinal cord retains high levels of oxidative modifications from samples of soluble lysate. Because we predict that oxidized SOD1 is a biomarker for the age of the protein, the lack of oxidative modifications in the SOD1 present in the aggregates may imply that an immature form of SOD1 is the actual substrate for aggregation.

Based on the findings presented here, we further speculate that zinc metallation occurs earlier than copper insertion,

which might displace a zinc ion already present in the copper site. We inferred the latter based on the trends of zinc metallation being inversely proportional to copper metallation among the different SOD1s (see the previous discussion section). Zinc binding may occur more rapidly than copper binding due to the stability it provides a folding monomer. Kinetic folding studies by Bruns and Kopito (71) revealed that hSOD1 requires tight zinc binding but not copper to reach a hyperstable state. The same study showed that forms of SOD1 with ALS-causing mutations generally tend to have slower overall kinetics of folding. The slower kinetics of mutant SOD1 folding potentially results in a higher sampling of off-pathway, aggregation-prone intermediates. This supports a mechanism in which mutant SOD1 aggregation is driven by nascently folded intermediates rather than a soluble mature protein. Based on these observations and our hypothesis that zinc metallation occurs early in the lifetime of SOD1, we speculate that the zinc acquisition step may be kinetically hindered in the folding mutant SOD1 polypeptides as compared with WT-SOD1. Additional experiments are needed to understand the specific mechanism of SOD1 metal acquisition and its potential implications for toxicity.

Metal Homeostasis—In our studies on metal distribution in the spinal cord, a major shift in copper levels observed in tissues from G93A and G37R spinal cords was also present in the hWT spinal cords. Thus, this effect is more likely due to SOD1 overexpression than to the disease. Nevertheless, it is intriguing that copper distributions are highly altered within these tissues, with a shifting of copper reflective of the same regions that have high SOD1 content despite the fact that the overall levels of copper in these tissues are unaltered relative to spinal cords of the NTG mice. It seems possible that high levels of SOD1 in some portions of these tissues make the other portions copper-deficient to some degree. This finding supports the idea that SOD1 plays a role in normal metal homeostasis. Interestingly, a recent study by Tokuda *et al.* (72) revealed that major alterations in copper homeostasis were associated with G93A hSOD1.

In our studies we found a statistically significant net increase in zinc associated with the white matter for the mutants H46R/H48Q, G37R, and G93A mice compared with the hWT and NTG controls. This is consistent with studies that have shown increased labile zinc in a G93A mouse spinal cord, increased levels of the zinc responsive metallothionein, and other general disturbances of zinc homeostasis in transgenic mouse spinal cords (24, 73–76). Similar but preliminary investigations using synchrotron micro x-ray fluorescence microscopy on sporadic ALS patients observed a marked increase in zinc in motor neurons (77). It is unclear why we observe the increased zinc in the white matter, when the motor neurons originate in the gray matter. One possible explanation may be the temporal nature of this study. A disease-relevant change in metal homeostasis for the gray matter may be masked by the downstream processes of neurodegeneration. For future experiments, it would be beneficial to investigate distributions of metals in tissues at earlier time points, especially right before and around the time when symptoms appear in the mice.

Conclusions—Metals have long been a "player of interest" in the search for the causes of ALS pathology, but until now their role has been very difficult to study as it was not possible to look at their distribution in tissues and specific proteins. The recent advent of powerful new analytical techniques has allowed us to address some of the relevant questions about the role of metals in ALS. Gentle SOD1 separation coupled to LC-ICP-MS has allowed us to determine precisely the amounts of metals bound to SOD1 molecules in different tissues, and synchrotron spectroscopy micro imaging techniques have allowed us to determine the micro distributions of selected metals within these tissues. These techniques have uncovered disease relevant changes in metallostasis in ALS-SOD1 transgenic mice that may be relevant to the human disease.

Acknowledgments—We thank Alvin Acerbo, Dr. Antonio Lanzirotti, Dr. Andreana Leskovjan, Randy Smith, and Dr. Ryan Tappero for help with beamline X27A and with data analysis on tissue cross-sections and Dr. Sadaf Sehati for editing and proofreading the manuscript. The National Synchrotron Light Source is supported by the United States Department of Energy under Contract DE-AC02-98CH10886.

REFERENCES

1. Cleveland, D. W. (1999) *Neuron* **24,** 515–520
2. Traynor, B. J., Codd, M. B., Corr, B., Forde, C., Frost, E., and Hardiman, O. M. (2000) *Arch. Neurol.* **57,** 1171–1176
3. Rosen, D. R., Siddique, T., Patterson, D., Figlewicz, D. A., Sapp, P., Hentati, A., Donaldson, D., Goto, J., O'Regan, J. P., and Deng, H. X. (1993) *Nature* **362,** 59–62
4. Shaw, B. F., and Valentine, J. S. (2007) *Trends Biochem. Sci.* **32,** 78–85
5. Spencer, P. S., Ludolph, A. C., and Kisby, G. E. (1992) *Ann. N.Y. Acad. Sci.* **648,** 154–160
6. Jusić, A., Ries, M., and Sostarko, M. (1992) *Neurol. Croat.* **41,** 213–226
7. Johnson, F. O., and Atchison, W. D. (2009) *Neurotoxicology* **30,** 761–765
8. Qureshi, M., Brown, R. H., Jr., Rogers, J. T., and Cudkowicz, M. E. (2008) *Open Neurol. J.* **2,** 51–54
9. Kamel, F., Umbach, D. M., Munsat, T. L., Shefner, J. M., Hu, H., and Sandler, D. P. (2002) *Epidemiology* **13,** 311–319
10. Armon, C., Kurland, L. T., Daube, J. R., and O'Brien, P. C. (1991) *Neurology* **41,** 1077–1084
11. Nagata, H., Miyata, S., Nakamura, S., Kameyama, M., and Katsui, Y. (1985) *J. Neurol. Sci.* **67,** 173–178
12. Praline, J., Guennoc, A. M., Limousin, N., Hallak, H., de Toffol, B., and Corcia, P. (2007) *Clin. Neurol. Neurosurg.* **109,** 880–883
13. Kihira, T., Mukoyama, M., Ando, K., Yase, Y., and Yasui, M. (1990) *J. Neurol. Sci.* **98,** 251–258
14. Pamphlett, R., McQuilty, R., and Zarkos, K. (2001) *Neurotoxicology* **22,** 401–410
15. Markesbery, W. R., Ehmann, W. D., Candy, J. M., Ince, P. G., Shaw, P. J., Tandon, L., and Deibel, M. A. (1995) *Neurodegeneration* **4,** 383–390
16. Ihara, Y., Nobukuni, K., Takata, H., and Hayabara, T. (2005) *Neurol. Res.* **27,** 105–108
17. Guatteo, E., Carunchio, I., Pieri, M., Albo, F., Canu, N., Mercuri, N. B., and Zona, C. (2007) *Neurobiol. Dis.* **28,** 90–100
18. Yoshimasu, F., Yasui, M., Yase, Y., Iwata, S., Gajdusek, D. C., Gibbs, C. J., Jr., and Chen, K. M. (1980) *Psychiatry Clin. Neurosci.* **34,** 75–82
19. Ostachowicz, B., Lankosz, M., Tomik, B., Adamek, D., Wobrauschek, P., Streli, C., and Kregsamer, P. (2006) *Spectrochim. Acta Part B At. Spectrosc.* **61,** 1210–1213
20. Trumbull, K. A., and Beckman, J. S. (2009) *Antioxid. Redox Signal.* **11,** 1627–1639

21. Broniatowski, M., and Dynarowicz-Łatka, P. P. (2009) *J. Phys. Chem. B* **113,** 4275–4283
22. Greene, B., D. D. (ed) (1990) *Microbial Oxygenic Photoautotrophs for Metal-ion Binding*, pp. 280–302, McGraw-Hill Inc., New York
23. Levenson, C. W. (2005) *Physiol. Behav.* **86,** 399–406
24. Bertoni-Freddari, C., Fattoretti, P., Casoli, T., Di Stefano, G., Giorgetti, B., and Balietti, M. (2008) *Exp. Gerontol.* **43,** 389–393
25. Cleveland, D. W., and Rothstein, J. D. (2001) *Nat. Rev. Neurosci.* **2,** 806–819
26. Rothstein, J. D. (2009) *Ann. Neurol.* **65,** S3–S9
27. Zetterström, P., Stewart, H. G., Bergemalm, D., Jonsson, P. A., Graffmo, K. S., Andersen, P. M., Brännström, T., Oliveberg, M., and Marklund, S. L. (2007) *Proc. Natl. Acad. Sci. U.S.A.* **104,** 14157–14162
28. Johnston, J. A., Dalton, M. J., Gurney, M. E., and Kopito, R. R. (2000) *Proc. Natl. Acad. Sci. U.S.A.* **97,** 12571–12576
29. Wang, J., Slunt, H., Gonzales, V., Fromholt, D., Coonfield, M., Copeland, N. G., Jenkins, N. A., and Borchelt, D. R. (2003) *Hum. Mol. Genet.* **12,** 2753–2764
30. Rodriguez, J. A., Valentine, J. S., Eggers, D. K., Roe, J. A., Tiwari, A., Brown, R. H., Jr., and Hayward, L. J. (2002) *J. Biol. Chem.* **277,** 15932–15937
31. Lepock, J. R., Arnold, L. D., Torrie, B. H., Andrews, B., and Kruuv, J. (1985) *Arch. Biochem. Biophys.* **241,** 243–251
32. Forman, H. J., and Fridovich, I. (1973) *J. Biol. Chem.* **248,** 2645–2649
33. Roe, J. A., Butler, A., Scholler, D. M., Valentine, J. S., Marky, L., and Breslauer, K. J. (1988) *Biochemistry* **27,** 950–958
34. Rodriguez, J. A., Shaw, B. F., Durazo, A., Sohn, S. H., Doucette, P. A., Nersissian, A. M., Faull, K. F., Eggers, D. K., Tiwari, A., Hayward, L. J., and Valentine, J. S. (2005) *Proc. Natl. Acad. Sci. U.S.A.* **102,** 10516–10521
35. Banci, L., Bertini, I., D'Amelio, N., Libralesso, E., Turano, P., and Valentine, J. S. (2007) *Biochemistry* **46,** 9953–9962
36. Ray, S. S., Nowak, R. J., Strokovich, K., Brown, R. H., Jr., Walz, T., and Lansbury, P. T., Jr. (2004) *Biochemistry* **43,** 4899–4905
37. DiDonato, M., Craig, L., Huff, M. E., Thayer, M. M., Cardoso, R. M., Kassmann, C. J., Lo, T. P., Bruns, C. K., Powers, E. T., Kelly, J. W., Getzoff, E. D., and Tainer, J. A. (2003) *J. Mol. Biol.* **332,** 601–615
38. Chattopadhyay, M., Durazo, A., Sohn, S. H., Strong, C. D., Gralla, E. B., Whitelegge, J. P., and Valentine, J. S. (2008) *Proc. Natl. Acad. Sci. U.S.A.* **105,** 18663–18668
39. Furukawa, Y., and O'Halloran, T. V. (2005) *J. Biol. Chem.* **280,** 17266–17274
40. Oztug, Durer, Z. A., Cohlberg, J. A., Dinh, P., Padua, S., Ehrenclou, K., Downes, S., Tan, J. K., Nakano, Y., Bowman, C. J., Hoskins, J. L., Kwon, C., Mason, A. Z., Rodriguez, J. A., Doucette, P. A., Shaw, B. F., and Selverstone, Valentine, J. (2009) *PLoS One* **4,** e5004
41. Banci, L., Bertini, I., Durazo, A., Girotto, S., Gralla, E. B., Martinelli, M., Valentine, J. S., Vieru, M., and Whitelegge, J. P. (2007) *Proc. Natl. Acad. Sci. U.S.A.* **104,** 11263–11267
42. Wang, J., Xu, G., Gonzales, V., Coonfield, M., Fromholt, D., Copeland, N. G., Jenkins, N. A., and Borchelt, D. R. (2002) *Neurobiol. Dis.* **10,** 128–138
43. Shaw, B. F., Lelie, H. L., Durazo, A., Nersissian, A. M., Xu, G., Chan, P. K., Gralla, E. B., Tiwari, A., Hayward, L. J., Borchelt, D. R., Valentine, J. S., and Whitelegge, J. P. (2008) *J. Biol. Chem.* **283,** 8340–8350
44. Ukeda, H., Maeda, S., Ishii, T., and Sawamura, M. (1997) *Anal. Biochem.* **251,** 206–209
45. Valentine, J. S., Doucette, P. A., and Zittin Potter, S. (2005) *Annu. Rev. Biochem.* **74,** 563–593
46. Winkler, D. D., Schuermann, J. P., Cao, X., Holloway, S. P., Borchelt, D. R., Carroll, M. C., Proescher, J. B., Culotta, V. C., and Hart, P. J. (2009) *Biochemistry* **48,** 3436–3447
47. Borchelt, D. R., Lee, M. K., Slunt, H. S., Guarnieri, M., Xu, Z. S., Wong, P. C., Brown, R. H., Jr., Price, D. L., Sisodia, S. S., and Cleveland, D. W. (1994) *Proc. Natl. Acad. Sci. U.S.A.* **91,** 8292–8296
48. Linder, M. C., and Hazegh-Azam, M. (1996) *Am. J. Clin. Nutr.* **63,** 797S-811S
49. Khandekar, R. N., Raghunath, R., and Mishra, U. C. (1987) *Sci. Total Environ.* **66,** 185–191
50. Banks, T. E., Tupper, R., Watts, R. W., and Wormall, A. (1954) *Nature* **173,** 348–349
51. Jou, M. Y., Hall, A. G., Philipps, A. F., Kelleher, S. L., and Lönnerdal, B. (2009) *J. Nutr.* **139,** 835–841
52. Aschner, M., Erikson, K. M., Herrero, Hernández, E., Hernández, E. H., and Tjalkens, R. (2009) *Neuromolecular. Med.* **11,** 252–266
53. Gellein, K., Garruto, R. M., Syversen, T., Sjøbakk, T. E., and Flaten, T. P. (2003) *Biol. Trace Elem. Res.* **96,** 39–60
54. Shafiq-ur-Rehman., and Chandra, O. (1984) *Bull Environ Contam. Toxicol.* **32,** 157–165
55. Kiaei, M., Bush, A. I., Morrison, B. M., Morrison, J. H., Cherny, R. A., Volitakis, I., Beal, M. F., and Gordon, J. W. (2004) *J Neurosci.* **24,** 7945–7950
56. Rajan, M. T., Jagannatha Rao, K. S., Mamatha, B. M., Rao, R. V., Shanmugavelu, P., Menon, R. B., and Pavithran, M. V. (1997) *J. Neurol. Sci.* **146,** 153–166
57. Yoshimasu, F., Yasui, M., Yase, Y., Uebayashi, Y., Tanaka, S., Iwata, S., Sasajima, K., Gajdusek, D. C., Gibbs, C. J., Jr., and Chen, K. M. (1982) *Psychiatry Clin. Neurosci.* **36,** 173–179
58. López-Alonso, M., Miranda, M., Castillo, C., Hernández, J., García-Vaquero, M., and Benedito, J. L. (2007) *Food Addit Contam* **24,** 943–954
59. Liu, H., Zhu, H., Eggers, D. K., Nersissian, A. M., Faull, K. F., Goto, J. J., Ai, J., Sanders-Loehr, J., Gralla, E. B., and Valentine, J. S. (2000) *Biochemistry* **39,** 8125–8132
60. Goto, J. J., Zhu, H., Sanchez, R. J., Nersissian, A., Gralla, E. B., Valentine, J. S., and Cabelli, D. E. (2000) *J. Biol. Chem.* **275,** 1007–1014
61. Wang, J., Xu, G., and Borchelt, D. R. (2002) *Neurobiol. Dis.* **9,** 139–148
62. Wang, J., Xu, G., Li, H., Gonzales, V., Fromholt, D., Karch, C., Copeland, N. G., Jenkins, N. A., and Borchelt, D. R. (2005) *Hum. Mol. Genet.* **14,** 2335–2347
63. Popescu, B. F., Robinson, C. A., Rajput, A., Rajput, A. H., Harder, S. L., and Nichol, H. (2009) *Cerebellum* **8,** 74–79
64. Pardo, C. A., Xu, Z., Borchelt, D. R., Price, D. L., Sisodia, S. S., and Cleveland, D. W. (1995) *Proc. Natl. Acad. Sci. U.S.A.* **92,** 954–958
65. Sahawneh, M. A., Ricart, K. C., Roberts, B. R., Bomben, V. C., Basso, M., Ye, Y., Sahawneh, J., Franco, M. C., Beckman, J. S., and Estévez, A. G. (2010) *J. Biol. Chem.* **285,** 33885–33897
66. Furukawa, Y., Torres, A. S., and O'Halloran, T. V. (2004) *EMBO J.* **23,** 2872–2881
67. Karch, C. M., Prudencio, M., Winkler, D. D., Hart, P. J., and Borchelt, D. R. (2009) *Proc. Natl. Acad. Sci. U.S.A.* **106,** 7774–7779
68. Nordlund, A., Leinartaite, L., Saraboji, K., Aisenbrey, C., Gröbner, G., Zetterström, P., Danielsson, J., Logan, D. T., and Oliveberg, M. (2009) *Proc. Natl. Acad. Sci. U.S.A.* **106,** 9667–9672
69. Strange, R. W., Antonyuk, S. V., Hough, M. A., Doucette, P. A., Valentine, J. S., and Hasnain, S. S. (2006) *J. Mol. Biol.* **356,** 1152–1162
70. Borchelt, D. R., Guarnieri, M., Wong, P. C., Lee, M. K., Slunt, H. S., Xu, Z. S., Sisodia, S. S., Price, D. L., and Cleveland, D. W. (1995) *J. Biol. Chem.* **270,** 3234–3238
71. Bruns, C. K., and Kopito, R. R. (2007) *EMBO J.* **26,** 855–866
72. Tokuda, E., Okawa, E., and Ono, S. (2009) *J. Neurochem.* **111,** 181–191
73. Smith, A. P., and Lee, N. M. (2007) *Amyotroph. Lateral Scler.* **8,** 131–143
74. Kim, J., Kim, T. Y., Hwang, J. J., Lee, J. Y., Shin, J. H., Gwag, B. J., and Koh, J. Y. (2009) *Neurobiol. Dis.* **34,** 221–229
75. Yao, X. (2009) *Neurotoxicology* **30,** 121–126
76. Sillevis Smitt, P. A., Mulder, T. P., Verspaget, H. W., Blaauwgeers, H. G., Troost, D., and de Jong, J. M. B. V. (1994) *Biol. Signals.* **3,** 193–197
77. Tomik, B., Chwiej, J., Szczerbowska-Boruchowska, M., Lankosz, M., Wójcik, S., Adamek, D., Falkenberg, G., Bohic, S., Simionovici, A., Stegowski, Z., and Szczudlik, A. (2006) *Neurochem. Res.* **31,** 321–331